Contents lists available at ScienceDirect

Arabian Journal of Chemistry

journal homepage: www.ksu.edu.sa

Original article

Design, synthesis of *N*-thianyl indole acetamide derivatives as potential plant growth regulator

Li Lei, Xu Tang, Wei Sun, Anjing Liao, Jian Wu *

State Key Laboratory of Green Pesticide, Key Laboratory of Green Pesticide and Agricultural Bioengineering, Ministry of Education, Center for R&D of Fine Chemicals of Guizhou University, Guiyang 550025, China

ARTICLE INFO

Keywords:
Indoleacetamide derivative
Synthesis
Plant growth regulation
Mechanism of action

ABSTRACT

The design, synthesis, and testing of acetamide derivatives containing indole structures (**C**) were carried out to determine their potential for regulating plant growth. The root growth of *Arabidopsis thaliana* was strongly inhibited by certain compounds, with compounds **C2**, **C4**, **C6**, and **C7** achieving a 100 % inhibitory rate at a concentration of 100 μM. The growth of lateral roots in *A. thaliana* was significantly promoted by compounds **C2** and **C6** at a concentration of 50 μM. Additionally, these compounds have been found to increase the expression of genes associated with lateral root development, including *IAA14*, *LAX3*, *AXR3*, *GH3.1*, *GH3.3*, and *BRU6*. These genes are involved in the auxin signaling pathway and IAA-amino synthase-related genes. In brief, these target compounds may be promising lead compounds for developing agents that can regulate plant growth.

1. Introduction

Phytohormones are essential for plant life processes, and the manipulation of phytohormones to achieve specific crop phenotypes has become a popular tool in agricultural production (Zhao et al., 2024). Exogenous phytohormones and their related compounds offer specific advantages over alternative agrochemical agents through their ability to enhance crop resistance to biotic and abiotic stresses, improve crop morphology, and increase crop yield (Rademacher, 2015). As a result, agricultural chemists have become interested in the chemical modification of phytohormones to discover valuable compounds (Frackenpohl et al., 2023).

Auxin has been identified through classical coleoptile bending tests and plays an integral role in seedling and root growth. Auxin affects plants throughout the entire process of plant growth and development, including gametogenesis, embryogenesis, seedling growth, vascular patterning, and flower development (Zhao, 2010). Exogenous auxin has many uses in agriculture, which can be used in tissue culture to stimulate rooting of cuttings, promote fruit setting, and thin fruit (Rademacher, 2015). Indole-3-acetic acid (IAA) is a heterocyclic monocarboxylic acid compound and is the predominant natural auxin. Its structure was identified in 1934. After that, agricultural chemists developed a large number of derivatives around the indole skeleton and evaluated their auxin activity (Nigović et al., 1996; Porter and Thimann, 1965; Thimann, 1958). However, the auxin compounds that have been widely used so far are still mainly IAA, naphthalene acetic acid (NAA) and 2,4-D.

Scientists have proposed various theories to guide the structural modification of highly active auxins. These theories include the two-point attachment theory (Two PA), the three-point attachment theory (Three PA), the separation charge theory (SCT), the conformational change theory (CCT), the physico-chemical influence of a boundary (PCIB), and others. However, each theory has its limitations. For example, the Two PA theory does not account for the reversibility of enzymatic processes, the Three PA theory does not consider benzoic acid derivatives, and SCT fails to explain multidimensional physiological phenomena related to auxins. Additionally, both CCT and PCIB also have their own constraints (Ferro et al., 2010).

Therefore, we attempted to modify IAA using the traditional drug development concept of backbone conversion and active fragment splicing to obtain analogues of auxin. The potential of indole compounds as plant growth regulators has been well-documented, and potential

Abbreviations: IAA, indole-3-acetic acid; Ac6c, 1-Aminocyclohexane carboxylic acid; DEGs, Differentially expressed genes; LBD, Lateral organ binding domain; SHY2, SHORT HYPOCOTYL 2; ARFs, Auxin-responsive factors; GATA, GATA transcription factor; PLA2, PECTIN LYASE2; EXP17, EXPASIN17; PG, Polygalacturonase; PAA, Phenylacetic acid.

* Corresponding author.
E-mail address: jwu6@gzu.edu.cn (J. Wu).

https://doi.org/10.1016/j.arabjc.2024.106082
Received 26 March 2024; Accepted 7 December 2024
Available online 10 December 2024

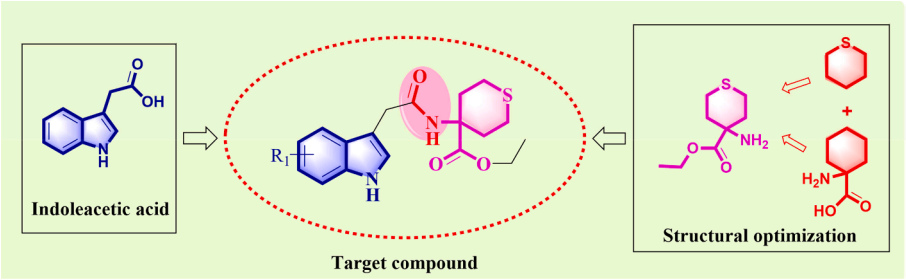

Fig. 1. Design of *N*-Thianyl indole acetamide derivatives.

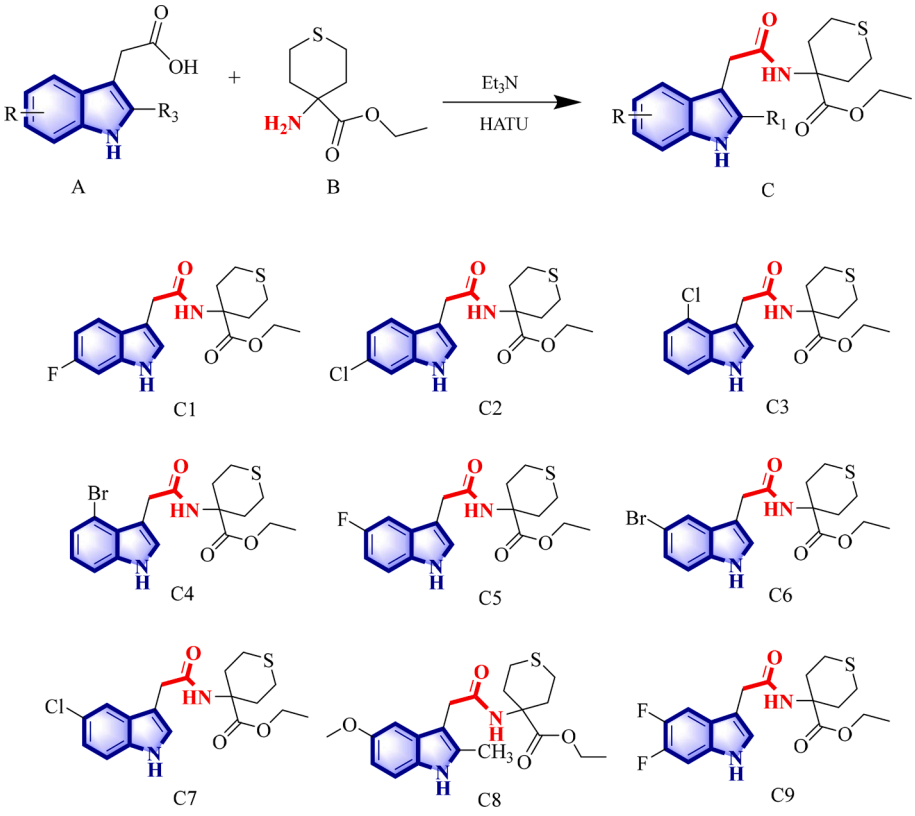

Scheme 1. The synthetic route of target compound **C** and the structures of **C1**–**C9.**

schemes for aminoacyl derivatization have been proposed (Sun et al., 2024, 2023). Tetrahydrothiopyran is a key six-membered ring system with a sulfur atom that has demonstrated potential in drug development. Compounds with this structure display diverse biological activities, including antimicrobial properties (Hada and Sharma, 2018; Łączkowski et al., 2016), anti-herpesvirus activity (Kontani et al., 2005), anticonvulsant activity (Łączkowski et al., 2016) and anti-bacterial infection treatment (Fu et al., 2014). Additionally, they have been used as phosphodiesterase inhibitors for cancer, diabetes, inflammation, psychiatric, and neurological disorders (Clauss et al., 2010), as well as potential penicillin-binding protein inhibitors (Rajalakshmi et al., 2020) and plant growth regulators (Kast et al., 1988). The sulfur atom found in this structure is noteworthy for its ability to improve compound selectivity and target adaptability (Beno et al., 2015). It functions as a potential hydrogen bond acceptor (Mustafa and Winum, 2022; Platts et al., 1996), making it a crucial and beneficial component in drug molecules.

Moreover, 1-aminocyclohexane carboxylic acid (Ac6c) is an important non-protein quaternary α-amino acid that plays a crucial role in the development of new drugs (Abercrombie et al., 2015). Certain compounds have displayed remarkable effects on plant growth regulation (Dejonghe et al., 2018; Vaidya et al., 2019). It was observed that some compounds exhibited promising anti-pest activity on plants in our previous work (Zhang et al., 2021).

After being inspired by the descriptions mentioned above, we aimed to create new non-protein quaternary α-amino acid derivatives containing sulfur by combining the structure of indole-3-acetic acid and tetrahydrothiopyran. This was achieved through a reaction involving the hydroxyl and amine groups to form an amide linker. The resulting compounds, *N*-thianyl indole acetamide derivatives (Fig. 1), were synthesized for potential use in regulating plant growth. Biological activity tests were carried out on these compounds to identify any that showed promising effects on plant growth regulation.

2. Materials and methods

2.1. Chemicals, reagents, and instrumentation

All reagents and solvents were purchased from commercial companies. The melting point of the compound was determined using an XT-4 micro melting point instrument from Beijing Tech Instrument Co.,

Table 1
Primer synthesis sequence.

Gene symbol	Forward	Reverse
IAA14	TGGGGAGTTATGGAGCACAAGGG	CACCAACGAGCATCCAGTCACC
LAX3	CGCCGTCACAGTGGAGATAATGC	GCGGATGGTAGCGTTAGCGTTAG
AXR3	GGGCAAACATGGAGGAGAAGAAGG	CGCCGACGAGCATCCAATCAC
GH 3.1	CTACGCAGACACAAGCACGATCC	CCAAGGCAGCAACGAGTCAGAG
GH3.3	CACGAGCCCTAACGAAGCCATC	ACGGAGGAGACCAGAAGCGAAG
BRU6	GGGTTCCATAATTCCGCTCCACAG	CAACCTCGACGCATTCTCCACTG
Actin	GGACACCGTAGCGAATCAATCAC	CGCGCCACAAAGAAGAAGTTTCATTAGG

Beijing, China. The NMR data of the synthesized compounds were recorded with a 400-MHz instrument (Bruker Advance III, Fallanden, Switzerland) or a JEOL-ECX 500 MHz (JEOL, Tokyo, Japan). High-resolution mass spectrometry (HRMS) data were conducted using an Orbitrap LC-MS instrument (Thermo Fisher Scientific, Waltham, MA, USA). The qRT-PCR kits were purchased from Sangon Biotech (Shanghai) Co., and the experiments were performed using a CFX96TM Real-Time System and an Eppendorf Centrifuge 5417R (Eppendorf AG, Hamburg, Germany). Additionally, we used a BIOBASE BBS-SDC Medical clean bench (Shandong Boke Regenerative Medicine Co., Ltd, Zaozhuang, China), an RXM type artificial climate box (Ningbo Jiangnan Instrument Factory, Ningbo, China), and a BIOBASE fully automatic autoclave (Shandong Boke Regenerative Medicine Co., Ltd, Zaozhuang, China) for our experiments.

$$Inhibitionrate(\%) = \frac{Rootlengthofcontrolgrowh - Rootlengthoftreatmentgrowth}{Rootlengthofcontrolgrowth} \times 100\%$$

2.2. Chemistry

As depicted in Scheme 1, compound **C** was easily obtained by reacting indole analogue A with ethyl 4-aminotetrahydro-2*H*-thiopyran-4-carboxylate in the presence of the condensing agent HATU.

2.3. Bio-activity

Different concentrations of compound solutions were prepared using DMSO as the solvent. The medium containing 10 μM IAA served as the positive control, while the medium containing a 0.1 % DMSO solution was used as the blank control. The DMSO content in the compound-treated group was consistent with that of the blank control group. *A. thaliana* was used for the study and the activity was tested at 100 μM for plant root growth. The experimental procedures were referenced from methods in the literature (Bai et al., 2021; Fendrych et al., 2018). *A. thaliana* plants were transplanted into the medium containing the compounds in groups of 6 plants, and 3 replicates were done for each compound. The original root length was marked, and the root length was measured after 10 days of growth. Each experiment was repeated three times.

Culture medium configuration. 1/2 Murashige & Skoog (MS) culture medium containing 0.8 % agar powder and with a pH of 5.8 was prepared. It was sterilized at 120 °C for 20 min. After sterilization, the culture medium was poured into 100 mm × 100 mm square culture dishes and allowed to cool and solidify.

Seed disinfection and cultivation. *A. Thaliana* seeds were first soaked in 70 % ethanol for 5 min., followed by a wash with 2.6 % sodium hypochlorite for 10 min. They were then rinsed 5–6 times with sterilized secondary water before being evenly distributed on the culture medium. Once sealed, the seeds were placed horizontally in an artificial climate box for 10 days to allow their true leaves to grow. The artificial climate box was programmed to a temperature of 21 °C, a humidity level of 67 % relative humidity, 16 h of light, and 8 h of darkness.

Root length test. A certain concentration of the compound was added to the culture medium and then poured into culture dishes, and left to solidify. Selected *A. thaliana* seedlings with uniform root length were transferred to culture dishes, and the initial root length was labeled. After sealing, they were placed vertically in an incubator and observed for growth. After 10 days, the root growth was observed and its length was recorded.

2.4. Molecular docking

The crystal structure of TIR1 (PDB ID: 2P1P) was obtained from the RCSB Protein Database(Tan et al., 2007). Molecular Operating Environment (MOE 2019) software was used to perform molecular docking. The preparation of TIR1 prior to docking was based on methods described in the literature (Wang et al., 2024). Docking was carried out with designed compounds and IAA, and the results were analyzed using MOE and PyMOL software tools.

2.5. Transcriptome analysis, molecular docking and qRT-PCR validation

The whole *A. thaliana* after 10 days of compound treatment was used as samples, and three experimental groups were selected for transcriptome sequencing analysis of compounds **C2** and **C6** at concentrations of 50 μM and 12.5 μM, respectively. The sequencing was done by Sangon Biotech (Shanghai) Co. The corresponding gene sequences were found in the NCBI database (https://www.ncbi.nlm.nih.gov) based on the gene ID. Primer design and synthesis were performed by Sangon Biotech (Shanghai) Co. The primer sequences are listed in Table 1. Functional categories were assigned through BLAST searches of the nonredundant GenBank database and by KEGG Pathway (http://www.genome.jp/kegg/) and Gene Ontology analysis (http://www.geneontology.org/).

A. thaliana plants were collected after 10 days of treatment with compounds **C2** and **C6**. The RNA was then extracted by grinding and mashing with liquid nitrogen. RNA was reverse transcribed to obtain cDNA, and actin was used as an internal reference gene for real-time fluorescence quantitative PCR. Three replicates were performed for each experiment and repeated three times. RNA was extracted using the Spin Column Plant Total RNA Purification Kit. Reverse transcription was performed using the M-MuLV First Strand cDNA Synthesis Kit. Detection was done using the SGExcel FastSYBR Mixture. Each experiment was repeated three times. The experimental data were processed using GraphPad Prism 9 software. The qRT-PCR experiments and calculations performed in this work followed the literature (Livak and Schmittgen,

Table 2
Inhibition of *A. thaliana* root growth by design compounds.[a]

Compound	Inhibition rate (%)			
	100 μM	50 μM	25 μM	12.5 μM
C1	74.18 ± 3.79	/	/	/
C2	100.00 ± 0.00	72.07 ± 2.52	43.48 ± 4.13	34.38 ± 3.21
C3	94.94 ± 1.53	41.51 ± 3.05	/	/
C4	100.00 ± 0.00	75.99 ± 4.66	9.04 ± 2.94	/
C5	71.49 ± 4.09	/	/	/
C6	100.00 ± 0.00	78.56 ± 2.63	36.87 ± 4.24	14.73 ± 2.58
C7	100.00 ± 0.00	50.18 ± 4.83	−0.27 ± 4.09	/
C8	46.94 ± 4.32	/	/	/
C9	60.31 ± 4.79	/	/	/
IAA[b]	100 ± 0.00	100 ± 0.00	100 ± 0.00	100 ± 0.00

The data in the table is the average value of three repetitions. ±standard error.
[a]The average of triplicate.
[b]Positive control in 10 μM.

2001). Details of the gene sequences for primer design were performed in the Supporting Information.

3. Results and discussion

3.1. Synthesis of target compounds

The synthetic route for the title compounds is shown in Scheme 1. Compound **A** and compound **B** were added to a round bottom flask and dissolved in acetonitrile. Triethylamine and the condensation agent HATU were added and the reaction was stopped after 3–4 h. The reaction solution was poured into water, stirred until a solid precipitated, filtered and dried to obtain the target compound **C**. The target compounds were structurally characterized using ^{1}H NMR, ^{13}C NMR, ^{19}F NMR, FT-IR, and HRMS. The NMR, HR-MS, and FT-IR spectra of the target compounds can be found in the Supporting Information. The physical and chemical properties of the target compound are as follows:

Ethyl 4-(2-(6-fluoro-1H-indol-3-yl) acetamido) tetrahydro-2H-thiopyran-4-carboxylate (C1). Yield 93.4 %; white powder; m.p. 134–136 °C. ^{1}H NMR (500 MHz, DMSO) δ: 10.93 (s, 1H, NH), 8.24 (s, 1H, NH), 7.54 (dd, J = 8.7, 5.5 Hz, 1H, Ar—H), 7.17 (d, J = 2.3 Hz, 1H, CH), 7.11 (dd, J = 10.2, 2.3 Hz, 1H, Ar—H), 6.84 (ddd, J = 9.8, 8.7, 2.4 Hz, 1H, Ar—H), 3.97 (t, J = 7.1 Hz, 2H, CH_2), 3.56 (s, 2H, CH_2), 2.78–2.72 (m, 2H, CH_2), 2.48–2.43 (m, 2H, CH_2), 2.21 (d, J = 16.1 Hz, 2H, CH_2), 1.94 (td, J = 11.1, 5.8 Hz, 2H, CH_2), 1.02 (t, J = 7.1 Hz, 3H, CH_3). ^{13}C NMR (126 MHz, DMSO) δ: 173.80, 171.07, 160.26, 158.40, 136.40 (d, J = 12.7 Hz), 124.76, 124.59, 120.22 (d, J = 10.3 Hz), 109.64, 107.30, 107.10, 97.85, 97.65, 60.83, 57.48, 33.37, 32.65, 23.08, 14.36. ^{19}F NMR (471 MHz, DMSO) δ: −122.20 (td, J = 9.9, 5.6 Hz). HR-MS (ESI): Calculated for $C_{18}H_{21}FN_2O_3S$ $[M + H]^+$: 365.13296, found: 365.13297; IR (KBr, cm^{-1}): ν 3383.67, 3240.82 (N–H), 1713.4, 1640.14 (C═O) cm^{-1}, 1553.60 (stretching vibration of indole skeleton).

Ethyl 4-(2-(6-chloro-1H-indol-3-yl) acetamido) tetrahydro-2H-thiopyran-4-carboxylate (C2). Yield 92.4 %; white powder; m.p. 146–147 °C. ^{1}H NMR (500 MHz, DMSO) δ: 11.00 (s, 1H, NH), 8.25 (s, 1H, NH), 7.56 (d, J = 8.5 Hz, 1H, Ar—H), 7.38 (d, J = 1.8 Hz, 1H, Ar—H), 7.22 (d, J = 2.3 Hz, 1H, Ar—H), 6.99 (dd, J = 8.4, 1.9 Hz, 1H, NH), 3.96 (t, J = 7.1 Hz, 2H, CH_2), 3.56 (s, 2H, CH_2), 2.76 (dd, J = 18.4,

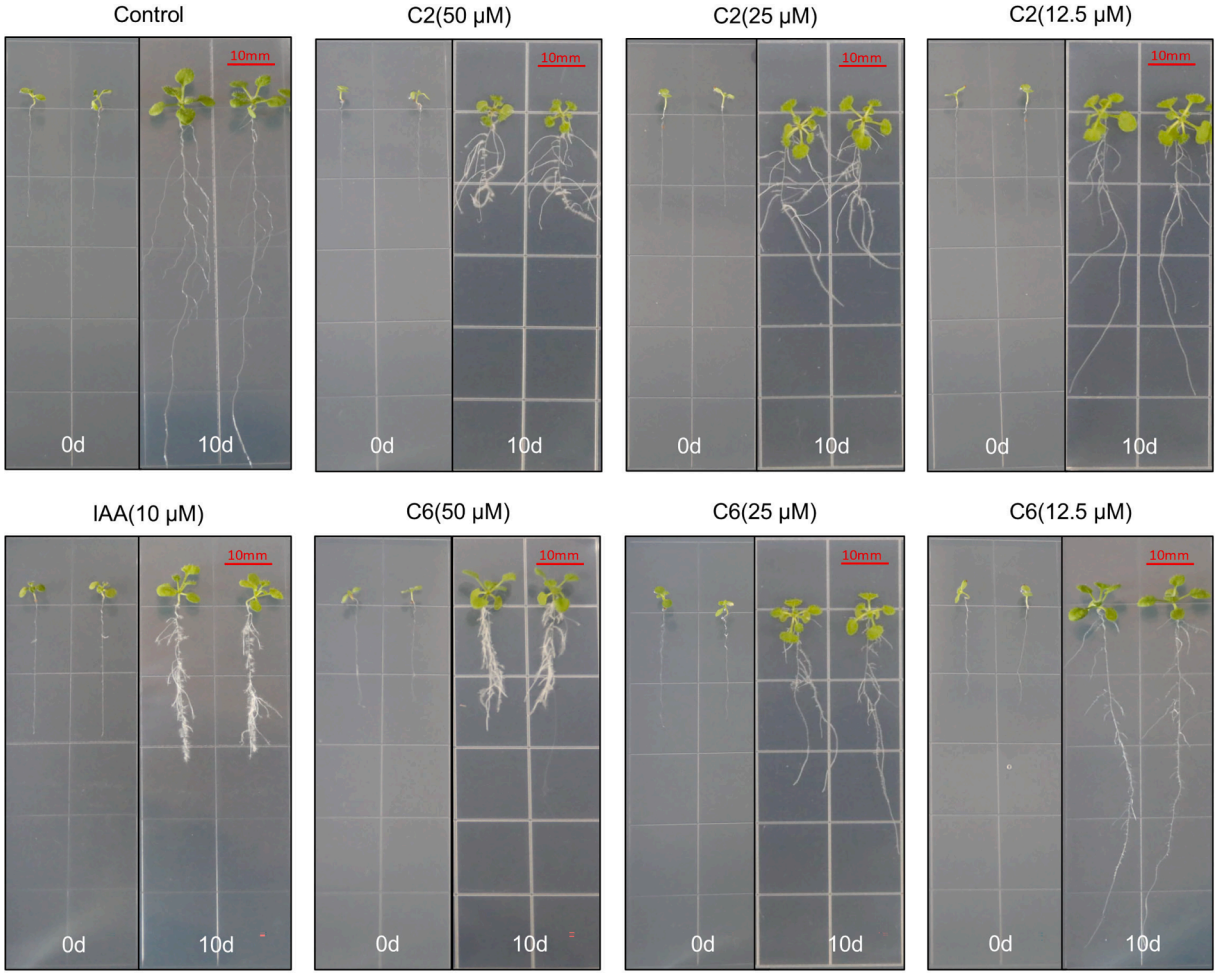

Fig. 2. Effects of compounds **C6** and **C2** on root growth of *A. thaliana* before (0 d) and after (10 d) treatment.

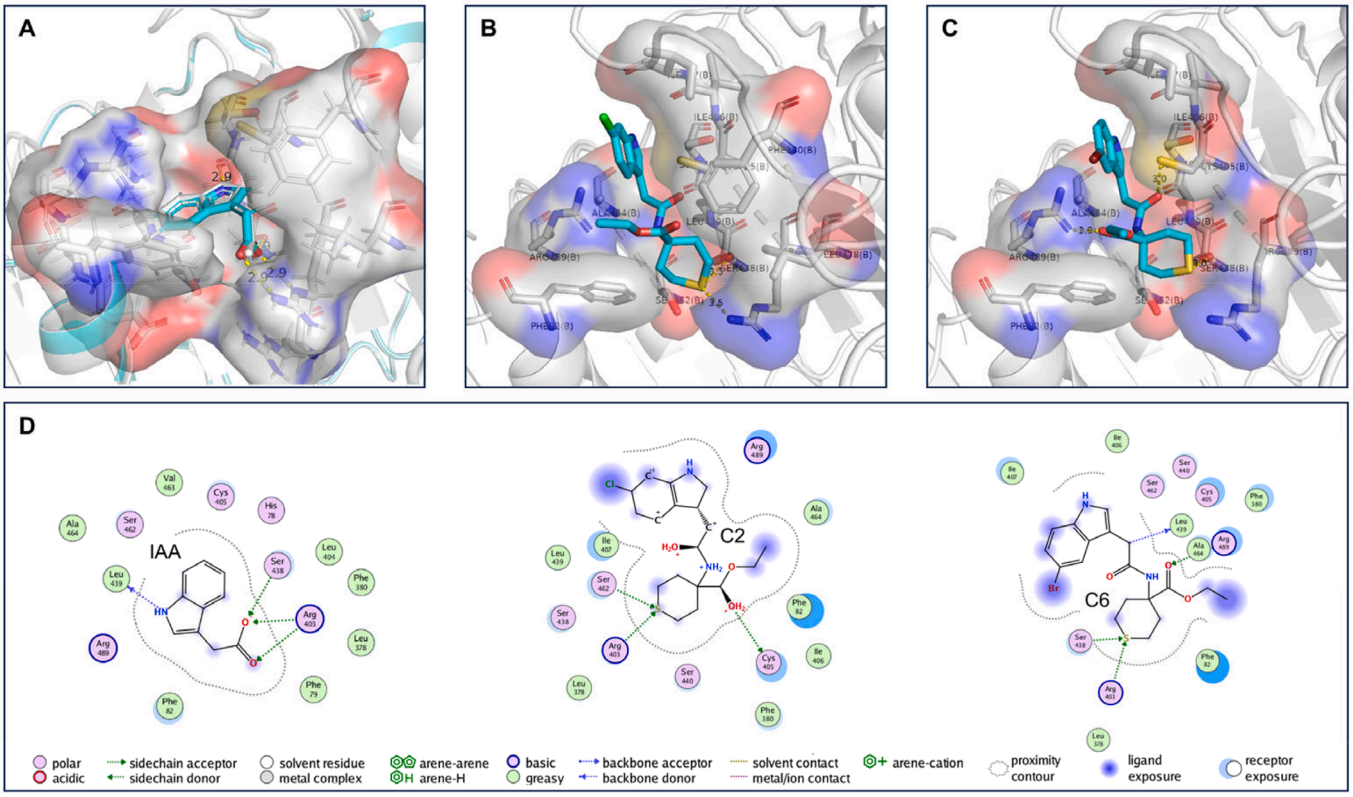

E

Ligand	IAA	IAA	IAA	IAA	IAA	C2	C2	C2	C2	C6	C6	C6	C6	C6	C6
Lig-Mol	N	O(2)	O(3)	O(3)	O(3)	O(3)	S	S	S	C(9)	O(3)	S	S	S	S
Residue	Leu439	Arg403	Arg403	Arg403	Ser438	Cys405	Arg403	Arg403	Ser462	Leu439	Arg489	Arg403	Arg403	Arg403	Ser438
Res-Mol	O	NH(2)	NE	NH(2)	OG	SG	NE	NH(2)	OG	O	NH(1)	CB	NE	NH(2)	OG
Interaction	H-donor	H-acceptor	H-acceptor	H-acceptor	H-acceptor	H-donor	H-acceptor	H-acceptor	H-acceptor	H-donor	H-acceptor	H-acceptor	H-acceptor	H-acceptor	H-acceptor
Distance	2.88	2.92	2.91	3.3	2.89	3.83	3.39	3.45	4.01	3.51	2.95	4.12	3.4	3.57	3.04
E(Kcal/mol)	-2.3	-7.2	-6.6	-0.9	-3.2	-2.2	-2.6	-3	-0.5	-0.8	-4.3	-0.5	-4.2	-3.8	-1.9

Fig. 3. Visualization of Molecular Docking results for TIR1. (**A**) The original protein 2P1P (including IAA) is shown in white, and the redocking IAA is shown in cyan. (**B**) TIR1 with **C2** docked into the binding pocket. (**C**) TIR1 with **C6** docked into the binding pocket. (**D**) The 2D interactions of IAA, **C2** and **C6** with TIR1, respectively. (E) The results of interaction between ligands and TIR1.

Table 3
The results of molecular docking.

Ligand	S	Rmsd_refine	E_conf	E_place	E_score1	E_refine	E_score2
IAA	−6.1992	1.8976	−53.9035	−58.7221	−11.6119	−37.5524	−6.1992
C1	−7.0980	2.3739	31.3360	−66.6915	−10.3555	−38.1116	−7.0980
C2	−7.1567	2.4197	28.2746	−56.3484	−9.1215	−38.8626	−7.1567
C3	−6.9773	0.8448	47.7374	−67.4063	−10.2848	−36.3680	−6.9773
C4	−6.9244	1.0847	56.6324	−53.0436	−9.0128	−34.7657	−6.9244
C5	−7.0944	1.5874	34.4199	−48.9477	−9.0196	−36.0892	−7.0944
C6	−7.1679	2.7296	25.7069	−70.9308	−9.4579	−40.2284	−7.1679
C7	−6.9384	2.3898	30.4306	−51.3474	−9.0779	−34.0082	−6.9384
C8	−6.8703	2.0527	21.0983	−44.7233	−9.7485	−33.6516	−6.8703
C9	−6.7764	1.3983	47.9787	−51.6302	−10.5733	−28.3215	−6.7764

S: The final score. **Rmsd_refine**: The mean square deviation between the laying refinement and after-refinement pose. **E_conf**: Energy conformer. **E_place**: Score for the ligand replacement phase. **E_score1**: The score of the first rescoring stage of generated poses. **E_refine**: The score of the refinement stage which use either the explicit molecular mechanics force field method or the grid-based energetics method. **E_score2**: The score of the final pose rescored using one of several scoring schemes (Behazin and Ebrahimi, 2018; Wahba et al., 2024).

6.9 Hz, 2H, CH_2), 2.48–2.44 (m, 2H, CH_2), 2.21 (d, J = 16.1 Hz, 2H, CH_2), 1.96–1.91 (m, 2H, CH_2), 1.02 (t, J = 7.1 Hz, 3H, CH_3). ^{13}C NMR (126 MHz, DMSO) δ: 173.78, 171.00, 136.95, 126.55, 126.20, 125.34, 120.62, 119.06, 111.44, 109.75, 60.84, 57.49, 33.36, 32.54, 23.08, 14.36. HR-MS (ESI): Calculated for $C_{18}H_{21}ClN_2O_3S$ $[M + H]^+$: 381.10341, found: 381.10342; IR (KBr, cm^{-1}): ν 3291.01 (N–H), 1727.01, 1646.63 (C═O), 1544.29 (stretching vibration of indole skeleton).

Ethyl 4-(2-(4-chloro-1H-indol-3-yl) acetamido) tetrahydro-2H-thiopyran-4-carboxylate (C3). Yield 94.3 %; white powder; m.p. 131–133 °C. ^{1}H NMR (500 MHz, DMSO) δ 11.23 (s, 1H, NH), 8.15 (s, 1H, NH), 7.32 (dd, J = 8.0, 0.7 Hz, 1H, Ar—H), 7.24 (d, J = 2.3 Hz, 1H,

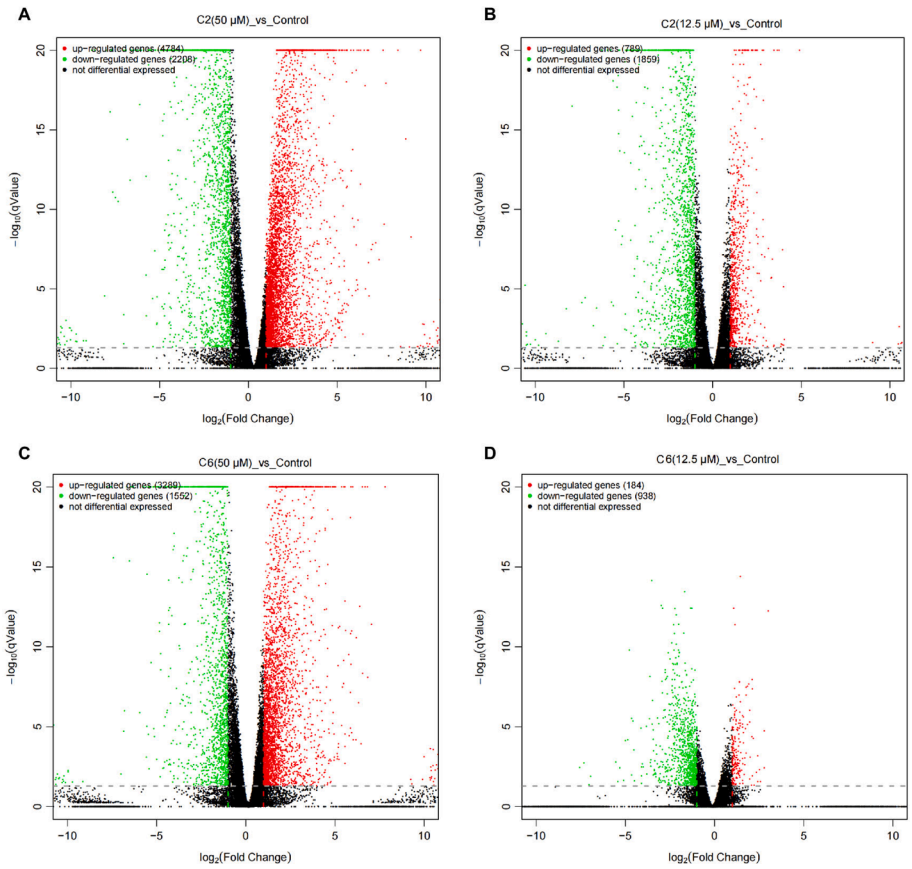

Fig. 4. Volcano maps of differentially expressed genes (DEGs) between the control group and the treatment groups (**C2** and **C6**). The DEGs were obtained by comparing the **C2** and **C6** treatments with control, and the criteria for the DEGs were $\log_2$ (fold change) ≥ 1 and false discovery rate < 0.05. **(A)** Comparison between compound **C2** at 50 μM treatment and control. **(B)** Comparison between compound **C2** at 12.5 μM treatment and control. **(C)** Comparison between compound **C6** at 50 μM treatment and control. **(D)** Comparison between compound **C6** at 12.5 μM treatment and control.

Ar—H), 7.02 (t, J = 7.8 Hz, 1H, CH), 6.96 (dd, J = 7.5, 0.6 Hz, 1H, Ar—H), 4.03 (q, J = 7.1 Hz, 2H, CH_2), 3.82 (s, 2H, CH_2), 2.86–2.80 (m, 2H, CH_2), 2.47 (t, J = 3.6 Hz, 2H, CH_2), 2.24 (d, J = 16.0 Hz), 2H, CH_2, 1.99–1.92 (m, 2H, CH_2), 1.13 (t, J = 7.1 Hz, 3H, CH_3). ^{13}C NMR (126 MHz, DMSO) δ 173.89, 171.26, 138.23, 126.55, 125.20, 124.32, 122.20, 119.59, 111.22, 109.03, 60.87, 57.50, 33.46 (d, J = 5.8 Hz), 23.14, 14.51. HR-MS (ESI): Calculated for $C_{18}H_{21}ClN_2O_3S$ $[M + H]^+$: 381.10341, found: 381.10342; IR (KBr, cm^{-1}): ν 3278.92 (N–H), 1724.77, 1647.00 (C═O), 1502.38 (stretching vibration of indole skeleton).

Ethyl 4-(2-(4-bromo-1H-indol-3-yl) acetamido) tetrahydro-2H-thiopyran-4-carboxylate (C4). Yield 93.6 %; white powder; m.p. 130–132 °C. ^{1}H NMR (500 MHz, DMSO) δ: 11.25 (s, 1H, NH), 8.15 (s, 1H, NH), 7.37 (dd, J = 7.9, 0.5 Hz, 1H, Ar—H), 7.26 (d, J = 2.4 Hz, 1H, Ar—H), 7.14 (dd, J = 7.5, 0.5 Hz, 1H, Ar—H), 6.96 (t, J = 7.8 Hz, 1H, CH), 4.04 (q, J = 7.1 Hz, 2H, CH_2), 3.85 (s, 2H, CH_2), 2.87–2.80 (m, 2H, CH_2), 2.48 (dd, J = 8.6, 4.7 Hz, 2H, CH_2), 2.27–2.22 (m, 2H, CH_2), 1.99–1.93 (m, 2H, CH_2), 1.14 (t, J = 7.1 Hz, 3H, CH_3). ^{13}C NMR (126 MHz, DMSO) δ: 173.89, 171.17, 138.05, 126.79, 123.02, 122.57, 113.47, 111.76, 109.61, 60.88, 57.52, 33.45 (d, J = 11.3 Hz), 23.19, 14.55. HR-MS (ESI): Calculated for $C_{18}H_{21}BrN_2O_3S$ $[M + H]^+$: 425.05290, found: 425.05290; IR (KBr, cm^{-1}): ν 3200.97 (N–H), 1731.28, 1652.52 (C═O), 1509.19 (stretching vibration of indole skeleton).

Ethyl 4-(2-(5-fluoro-1H-indol-3-yl) acetamido) tetrahydro-2H-thiopyran-4-carboxylate (C5). Yield 91.3 %; white powder; m.p. 137–138 °C. ^{1}H NMR (500 MHz, DMSO) δ: 10.96 (s, 1H, NH), 8.26 (s, 1H, NH), 7.32 (dt, J = 9.9, 4.2 Hz, 1H, Ar—H), 7.24 (d, J = 2.3 Hz, 1H, NH), 6.90 (td, J = 9.2, 2.5 Hz, 2H, Ar—H), 3.96 (q, J = 7.1 Hz, 2H, CH_2), 3.54 (s, 2H, CH_2), 2.79–2.73 (m, 2H, CH_2), 2.49–2.44 (m, 2H, CH_2), 2.25–2.19 (m, 2H, CH_2), 1.97–1.90 (m, 2H, CH_2), 1.01 (t, J = 7.1 Hz, 3H, CH_3). ^{13}C NMR (126 MHz, DMSO) δ: 173.79, 171.07, 133.27, 127.94 (d, J = 10.0 Hz), 126.33, 112.72 (d, J = 9.8 Hz), 109.67 (d, J = 5.0 Hz), 109.43, 103.88, 60.81, 57.49, 33.37, 32.67, 23.08, 14.30. ^{19}F NMR (471 MHz, DMSO) δ: −125.47 (dd, J = 24.2, 13.1 Hz). HR-MS (ESI): Calculated for $C_{18}H_{21}FN_2O_3S$ $[M + H]^+$: 365.13296, found: 365.13297; IR (KBr, cm^{-1}): ν 3355.51 (N–H), 1712.69, 1640.88 (C = O), 1553.85 (stretching vibration of indole skeleton).

***Ethyl 4-(2-(5-bromo-1H-indol-3-yl) acetamido) tetrahydro-2H-thiopyran-4-carboxylate* (C6).** Yield 91.6 %; brown solid; m.p. 82–84 °C. ^{1}H NMR (500 MHz, DMSO) δ: 11.07 (s, 1H, NH), 8.28 (s, 1H, NH), 7.77 (d, J = 1.8 Hz, 1H, Ar—H), 7.32 (s, 1H, NH), 7.23 (d, J = 2.3 Hz, 1H, Ar—H), 7.17 (dd, J = 8.6, 1.9 Hz, 1H, Ar—H), 3.98–3.94 (m, 2H, CH_2), 3.55 (s, 2H, CH_2), 2.80–2.74 (m, 2H, CH_2), 2.49–2.44 (m, 2H, CH_2), 2.24–2.19 (m, 2H, CH_2), 1.96–1.90 (m, 2H, CH_2), 0.99 (t, J = 7.1 Hz, 3H, CH_3). ^{13}C NMR (126 MHz, DMSO) δ: 173.78, 171.00, 135.30, 129.55, 125.95, 123.86, 121.77, 113.82, 111.51, 109.26, 60.82, 57.50, 33.37, 32.56, 23.10, 14.34. HR-MS (ESI): Calculated for $C_{18}H_{21}BrN_2O_3S$ $[M + H]^+$: 425.05290, found: 425.05290; IR (KBr, cm^{-1}): ν 3287.29 (N–H), 1723.20, 1649.20 (C═O), 1513.27 (stretching vibration of indole skeleton).

Ethyl 4-(2-(5-chloro-1H-indol-3-yl) acetamido) tetrahydro-2H-thiopyran-4-carboxylate (C7). Yield 89.6 %; brown solid; m.p. 112–114 °C. ^{1}H NMR (500 MHz, DMSO) δ: 11.06 (s, 1H, NH), 8.28 (s, 1H, NH), 7.62 (d, J = 2.0 Hz, 1H, Ar—H), 7.35 (d, J = 8.6 Hz, 1H, Ar—H), 7.25 (d, J = 2.3 Hz, 1H, NH), 7.05 (dd, J = 8.6, 2.1 Hz, 1H, Ar—H), 3.95 (q, J = 7.1 Hz, 2H, CH_2), 3.56 (s, 2H, CH_2), 2.81–2.74 (m, 2H, CH_2), 2.49–2.40 (m, 2H, CH_2), 2.22 (d, J = 15.9 Hz, 2H, CH_2),

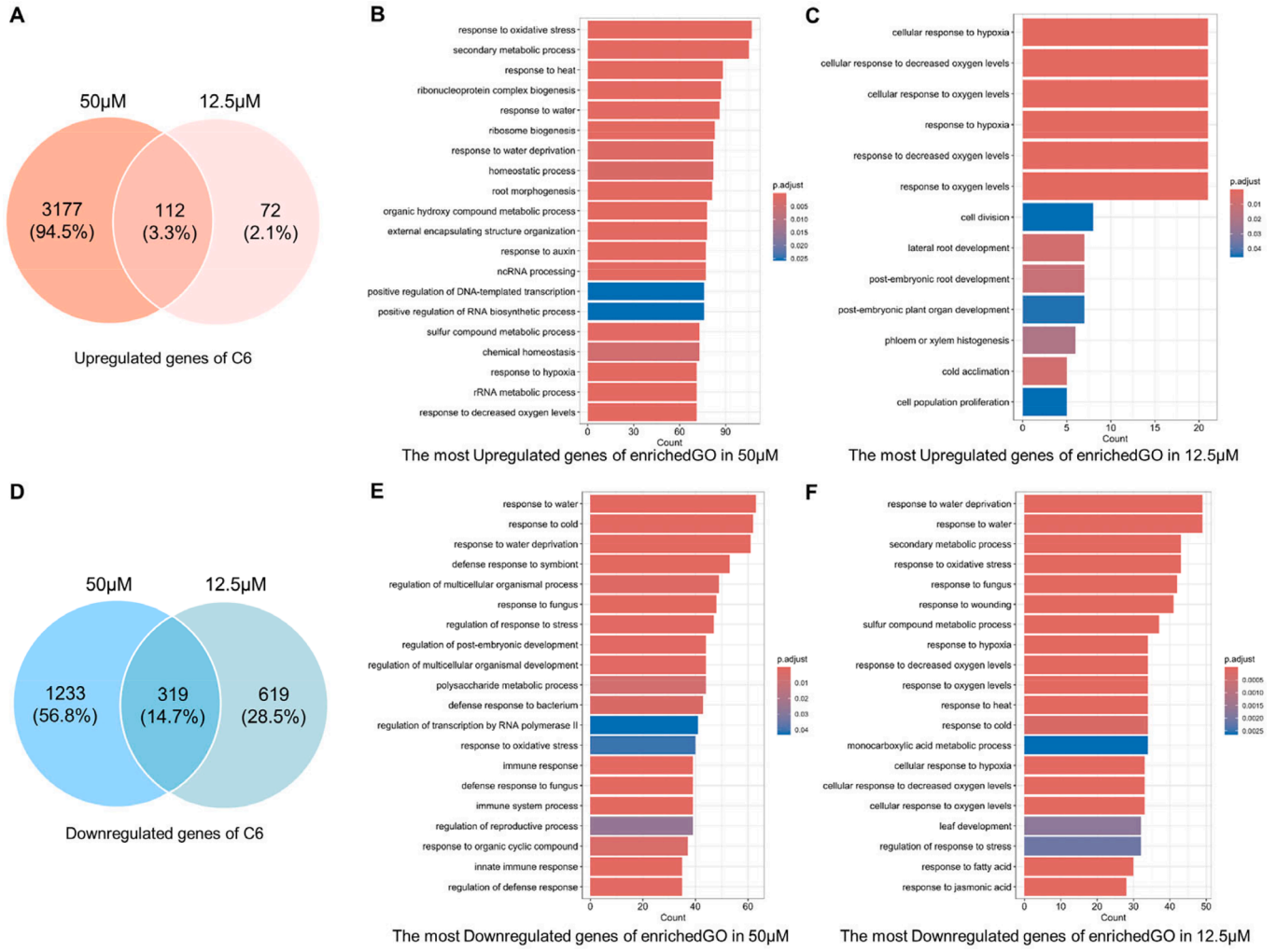

Fig. 5. The similarity and differences in the transcriptional profiles in the treatment of **C6**. (**A**) and (**D**) The comparison of DEGs at high and low concentrations of **C6**. (**B**) and (**E**) The Biological Process results of Gene Ontology (GO) enrichment for **C6** in 50 μM. (**C**) and (**F**) The Biological Process results of Gene Ontology (GO) enrichment for **C6** in 12.5 μM.

1.97–1.90 (m, 2H, CH_2), 0.99 (t, J = 7.1 Hz, 2H, CH_3). ^{13}C NMR (126 MHz, DMSO) δ: 173.78, 171.02, 135.07, 128.85, 126.11, 123.52, 121.35, 118.72, 113.34, 109.35, 60.81, 57.50, 33.37, 32.57, 23.09, 14.31. HR-MS (ESI): Calculated for $C_{18}H_{21}ClN_2O_3S$ $[M + H]^+$: 381.10341, found: 381.10342; IR (KBr, cm^{-1}): ν 3395.66 (N–H), 1721.77, 1641.11 (C═O), 1538.26 (stretching vibration of indole skeleton).

Ethyl 4-(2-(5-methoxy-2-methyl-1H-indol-3-yl) acetamido) tetrahydro-2H-thiopyran-4-carboxylate (C8). Yield 94.6 %; brown powder; m.p. 181–182 °C. ^{1}H NMR (500 MHz, DMSO) δ: 10.59 (s, 1H, NH), 8.20 (s, 1H, NH), 7.09 (t, J = 6.0 Hz, 2H, Ar—H), 6.60 (dd, J = 8.6, 2.5 Hz, 1H, Ar—H), 3.97 (q, J = 7.1 Hz, 2H, CH_2), 3.75 (s, 3H, CH_3), 3.47 (s, 2H, CH_2), 2.76 (dd, J = 19.2, 7.4 Hz, 2H, CH_2), 2.44–2.40 (m, 2H, CH_2), 2.31 (s, 3H, CH_3), 2.22 (d, J = 15.0 Hz, 2H, CH_2), 1.92–1.86 (m, 2H, CH_2), 1.04 (t, J = 7.1 Hz, 3H, CH_3). ^{13}C NMR (126 MHz, DMSO) δ: 173.88, 171.42, 153.44, 134.15, 130.55, 129.21, 111.34, 110.19, 105.44, 100.69, 60.81, 57.46, 55.71, 33.25, 31.66, 23.00, 14.37, 12.04. HR-MS (ESI): Calculated for $C_{20}H_{26}N_2O_4S$ $[M + H]^+$: 391.16860, found: 391.16860; IR (KBr, cm^{-1}): ν 3255.10 (N–H), 1734.59, 1663.12 (C═O), 1521.28 (stretching vibration of indole skeleton).

Ethyl 4-(2-(5,6-dibromo-1H-indol-3-yl) acetamido) tetrahydro-2H-thiopyran-4-carboxylate (C9). Yield 91.5 %; light brown powder; m.p. 159–160 °C. ^{1}H NMR (500 MHz, DMSO) δ: 11.03 (s, IH, NH), 8.27 (s, 1H, NH), 7.52 (dd, J = 11.5, 8.1 Hz, 1H, Ar—H), 7.34 (dd, J = 11.3, 7.0 Hz, 1H, Ar—H), 7.24 (d, J = 2.2 Hz, 1H, Ar—H), 3.95 (q, J = 7.1 Hz, 2H, CH_2), 3.54 (s, 2H, CH_2), 2.79–2.72 (m, 2H, CH_2), 2.49–2.44 (m, 2H, CH_2), 2.25–2.19 (m, 2H, CH_2), 1.97–1.90 (m, 2H, CH_2), 1.00 (t, J = 7.1 Hz, 3H, CH_3). ^{13}C NMR (126 MHz, DMSO) δ: 173.76, 170.93, 131.54 (d, J = 10.6 Hz), 126.20, 123.11 (d, J = 7.9 Hz), 109.93, 105.89 (d, J = 18.8 Hz), 99.59, 60.82, 57.50, 33.35, 32.63, 23.06, 14.27. ^{19}F NMR (471 MHz, DMSO) δ: −145.57 to −145.89 (m), −149.27 (ddd, J = 17.3, 11.1, 5.7 Hz). HR-MS (ESI): Calculated for $C_{18}H_{20}F_2N_2O_3S$ $[M + H]^+$: 383.12354, found: 383.12355; IR (KBr, cm^{-1}): ν 3338.93 (N—H), 1709.31, 1642.05 (C═O), 1521.28 (stretching vibration of indole skeleton).

3.2. *The activity for inhibition of root length*

The inhibition of *A. thaliana* root length was tested in a stepwise manner (Table 2). Initially, all compounds were tested at a concentration of 100 μM. It was found that all nine compounds exhibited inhibitory activity on the root length of *A. thaliana*. Specifically, compounds **C2**, **C3**, **C4**, **C6**, and **C7** exhibited showed over 90 % inhibition of root growth at 100 μM, which was comparable to the inhibition rate of IAA at 10 μM. To further investigate the effects of these compounds, the concentration of **C2**, **C3**, **C4**, **C6**, and **C7** was reduced to 50 μM and tested. At this concentration, compounds **C2**, **C4**, and **C6** demonstrated inhibition rates of 72.07 %, 75.99 %, and 78.56 %, respectively. Compounds **C2**,

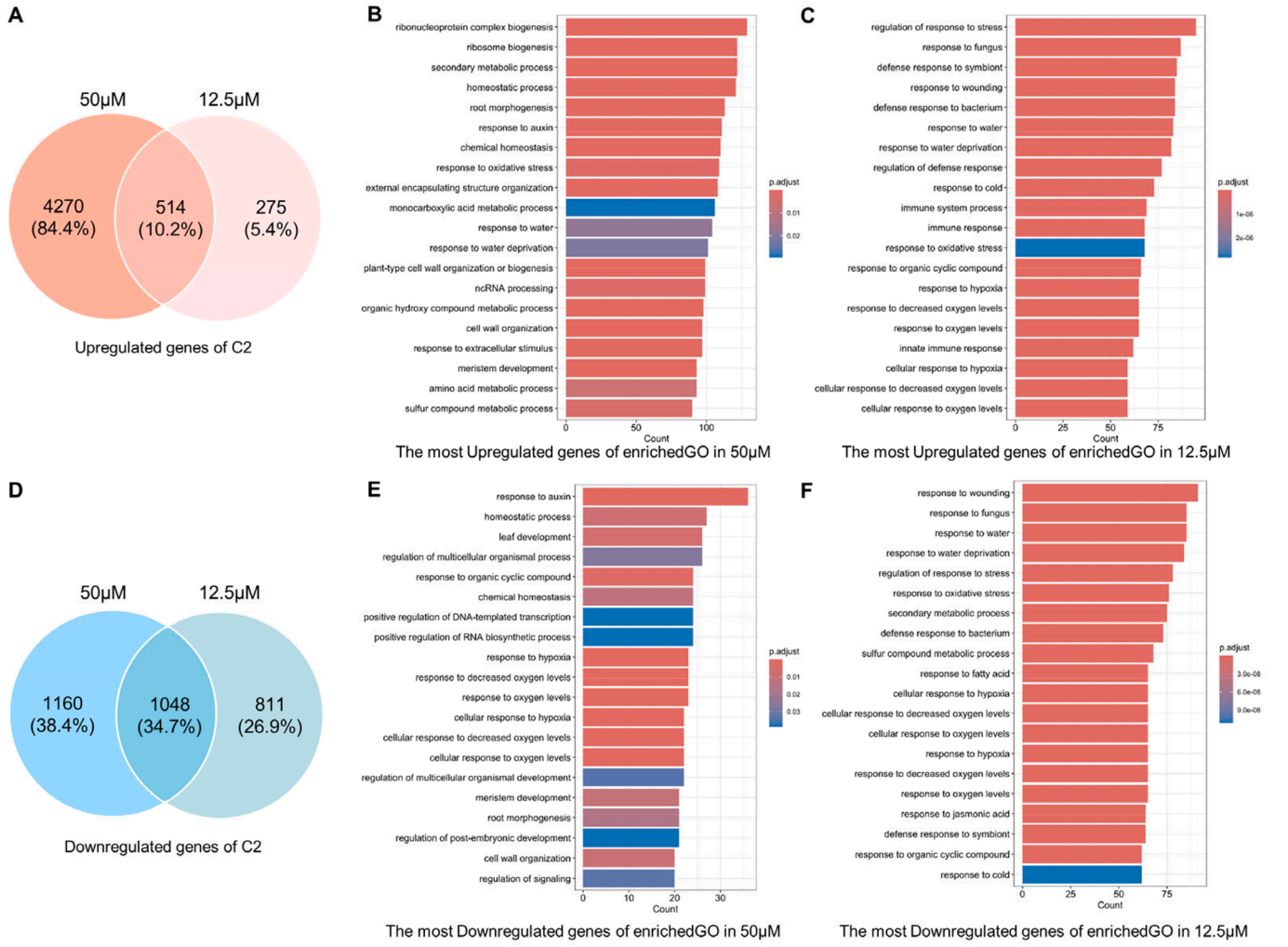

Fig. 6. The similarity and differences in the transcriptional profiles in the treatment of **C2**. (**A**) and (**D**) The comparison of DEGs at high and low concentrations of **C2**. (**B**) and (**E**) The Biological Process results of Gene Ontology (GO) enrichment for **C2** in 50 μM. (**C**) and (**F**) The Biological Process results of Gene Ontology (GO) enrichment for **C2** in 12.5 μM.

C3, and **C7** are indoles substituted with chlorine at the 6th, 4th, and 5th positions, respectively. On the other hand, compounds **C4** and **C6** are indoles with bromine substitutions at the 4th and 5th positions. Meanwhile, compounds **C1**, **C5**, and **C9** contain fluorine substitutions, and **C8** is an indole acetamide with a methoxy substitution. The results indicate that chlorine and bromine substitutions in indole derivatives exhibit higher activity compared to fluorine and methoxy substitutions.

Compounds **C2** and **C6** were particularly effective in inhibiting the growth of *A. thaliana* and significantly impacting its lateral root growth (Fig. 2). The primary root length of *A. thaliana* treated with 10 μM IAA stopped growing and showed lateral root and hair root development. **C2** and **C6** had similar effects at 50 μM, and their inhibition of root length decreased with decreasing concentration. The fact that IAA can enhance root growth at low concentrations while inhibiting root growth at high concentrations is widely recognized. The effects of these compounds, which have structures based on the modified structure of IAA, suggest a possible correlation with the mechanism of auxin action.

3.3. Molecular docking analysis

The auxin receptor TIR1 was used to perform molecular docking. IAA was re-docked and its position was almost consistent with the original ligand, indicating the reliability of the software environment for docking (Fig. 3**A**). The results in Table 3 showed that modifying the side chain of the indole ring improved the ligand's binding potential. The final scores (S) for **C6** and **C2** were −7.1679 and −7.1467, respectively. **C6** had the lowest conformationally optimized energy score (E_refine) of −40.2284, followed by **C2**. These two key indicators suggest that **C6** and **C2** have the best binding potential based on molecular docking for TIR1.

The 2D interactions between ligands and TIR1 demonstrate the effect of structural modifications of IAA on TIR1 (Fig. 3**D**). In **C2** and **C6**, sulfur atoms replace the carboxyl group of IAA and form hydrogen interactions with Arg and Ser. Arg403, Ser438, and Leu439 interact with IAA, while Arg403, Cys405, and Leu489 interact with **C2**. The amino acid residues that form hydrogen interactions with **C6** are Arg403, Ser438, Leu439, and Arg489. In general, the lower the energy, the more stable it is. The hydrogen interaction distances of **C2** and **C6** are greater than those of IAA, resulting in their higher energy compared to IAA (Fig. 3**E**). Additionally, the indole rings of **C2** and **C6** are pushed to the outside of the pocket (Fig. 3**B and C**) and occupy the amino acid positions of AUX/IAA7 in the bound state with TIR1, which would result in AUX/IAA7 being pushed away from **C2** and **C6**, making AUX/IAA7 less closely related to TIR1. These factors may be the reason why *A. thaliana* is less sensitive to **C2** and **C6** than to IAA.

3.4. Gene response analysis

To further explore the potential mechanisms of action of **C2** and **C6**,

Table 4
Differential gene expression in the auxin pathway of compounds **C2** and **C6**.[a]

Gene ID (symbol)	**C2** effect		**C6** effect		Gene function
	50 μM	12.5 μM	50 μM	12.5 μM	
AT1G77690-LAX3	–	–	Up	–	Auxin influx carrier; promotes lateral root germination
AT4G14550-IAA14	Up	–	Up	–	Participate in lateral root development
AT1G04250-AXR3	Up	–	Up	–	Involved in auxin signaling
AT4G32280-IAA29	Down	–	Down	–	Auxin induced protein
AT2G01200-IAA32	Down	–	–	–	Belongs to the auxin-inducible gene family
AT2G14960-GH3.1	Up	–	Up	–	Encodes a protein similar to IAA-amine synthase
AT2G23170-GH3.3	Up	–	–	–	Encodes an IAA-amino synthetase
AT4G37390-BRU6	Up	–	–	–	Encodes an IAA-amino synthetase
AT4G03400-DFL2	Down	Down	Down	–	Encoding *GH3*-related genes
AT1G48660-F11I4.15	–	–	Up	–	Auxin-responsive *GH3* family proteins
AT4G31320-SAUR37	Up	–	Up	–	Auxin responsive gene
AT3G09870-SAUR48	–	Up	Up	Up	Auxin responsive gene
AT2G21210-SAUR6	–	–	Up	–	Auxin responsive gene
AT2G37030-SAUR46	–	–	Up	Up	Auxin responsive gene
AT3G12830-SAUR72	–	–	Up	Up	Auxin responsive gene
AT2G28085-SAUR42	Down	–	Down	–	Auxin responsive gene
AT5G18050-SAUR22	Down	–	Down	–	Auxin responsive gene
AT4G22620-SAUR34	–	–	Down	Down	Auxin responsive gene

[a] The chosen thresholds was $|\mathrm{Log_2Fold}| \geq 2$.

a transcriptome analysis was performed on *A. thaliana* that treated with these compounds. Consistent with the results observed in Fig. 2, high concentrations of the compounds inhibited *A. thaliana* roots more strongly than low concentrations, resulting in a greater number of differentially expressed genes (DEGs). Treatment with 50 μM of compound **C2** resulted in the up-regulation of 4784 genes and the down-regulation of 2208 genes (Fig. 4**A**). Treatment with 12.5 μM of compound **C2** led to the up-regulation of 789 genes and the down-regulation of 1859 genes (Fig. 4**B**). Treatment with 50 μM of compound **C6** resulted in the up-regulation of 3289 genes and the down-regulation of 1552 genes (Fig. 4**C**). Treatment with 12.5 μM of compound **C6** led to the up-regulation of 184 genes and the down-regulation of 938 genes (Fig. 4**D**).

In general, we would assume that most of the genes induced by a low concentration should be part of the genes induced by a high concentration. However, the number of uniformly regulated genes in high and low concentrations was not overwhelmingly dominant (Fig. 5**A and C**, Fig. 6**A and C**). Out of the 184 genes up-regulated at a low **C6** concentration, 112 were also up-regulated at a high **C6** concentration, while only 319 of the 938 down-regulated genes were down-regulated at a high **C6** concentration. The number of DEGs after **C2** treatment was higher than that of **C6**. Out of the 789 genes up-regulated at a low concentration of **C2**, 514 genes were also up-regulated at a high concentration, and 1048 of the 1859 down-regulated genes were also down-regulated at high concentrations.

The biological processes enriched in GO were used to further reveal the changes within *A. thaliana* caused by compound treatment. As shown in Fig. 5**B and E**, the up-regulated DEGs by **C6** at 50 μM are enriched in multiple processes that respond to environmental changes, such as oxygen, temperature, and water. Changes in secondary metabolites, RNA and proteins are bound to occur. The responses of roots and auxin are important because they match the phenotype in Fig. 2. Corresponding to these, the down-regulated DEGs are mainly concentrated in plant resistance to biotic and abiotic stresses. As an active factor regulating plant growth, auxin can antagonize plant stress response (Zhao et al., 2024). These pieces of evidence suggest that the *A. thaliana* reaction treated with **C6** at 50 μM is closely related to auxin. No dramatic root changes are observed in *A. thaliana* treated with lower concentrations of **C6** (Fig. 2), so the number of up-regulated DEGs is much smaller (Fig. 5**C and F**). Significantly, the down-regulated DEGs were still heavily enriched in plant response to stress. This means that **C6**, as a potential chemical signal, is still sensed by plants and initiates inhibition of stress responses. *A. thaliana* treated with **C2** at 50 μM induces a more pronounced auxin response and root development (Fig. 6**B and E**), while a low concentration of **C2** is more prominent in stimulating plant stress responses (Fig. 6**C and F**).

The details of differentially expressed genes (DEGs) in response to auxin are presented in Table 4. The results revealed the presence of well-known genes such as *LAX3*, *AXR3*, and *IAA14*, as well as auxin metabolism-related genes *GH3.1*, *GH3.3*, and *BRU6*, all of which are associated with lateral root growth. The plant hormone IAA primarily regulates the expression of members of the *Aux/IAA* family of transcriptional regulators. The transcriptional regulation of auxin-responsive genes relies on two related families of transcriptional regulators: auxin-responsive factors (ARFs) and auxin/indole-3-acetic acid (*Aux/IAAs*). Specifically, ARF7 and ARF19 have been found to directly activate *A. thaliana LBD/ASL* genes, which play a crucial role in lateral root formation.

3.5. QRT-PCR analysis

The QRT-PCR validation of genes associated with lateral root development (Fig. 7). The qRT-PCR analysis results depicted in Fig. 7**A** indicate that compounds **C2** and **C6** significantly increased the expression of the *IAA14* gene at both concentrations of 50 μM and 12.5 μM. *IAA14* is a key factor in the initiation of lateral root growth in *A. thaliana* and also regulates the maturation stage of lateral root development (Guseman et al., 2015; Zhang et al., 2023). As shown in Fig. 8, the expression of GATA23 (a GATA transcription factor) and LBD16 (a Lateral Organ Binding Domain), which play important roles in lateral root growth, is influenced by *IAA28* and *IAA14*, respectively (Lavenus et al., 2013; Li et al., 2022). SLR/IAA14 is a key regulator of growth hormone-regulated growth and development, particularly in lateral root formation (Fukaki et al., 2002). In slr-mutants, the stabilized mutant *IAA14* protein inactivates ARF7/ARF19 function, thereby blocking lateral root formation in these mutants (Fukaki et al., 2005). It is evident that *IAA14* interacts with other regulatory factors to govern lateral root growth and development.

The regulation of root growth and development is dependent on the *LAX3* gene, which controls the influx of auxin. Notably, compounds **C2** and **C6** were discovered to markedly enhance the expression of the *LAX3* gene (Fig. 7**B**). As shown in Fig. 8, *LAX3* is specifically expressed near lateral root primordia and regulates the expression of cell wall remodeling proteins such as Pectin Lyase 2 (PLA 2), polygalacturonase (PG), and EXPASIN17 (EXP17). These proteins are involved in breaking down demethylated pectin in the cell wall (Cosgrove, 2000; Marín-Rodríguez et al., 2002). Increased *LAX3* activity promotes the induction of cell wall

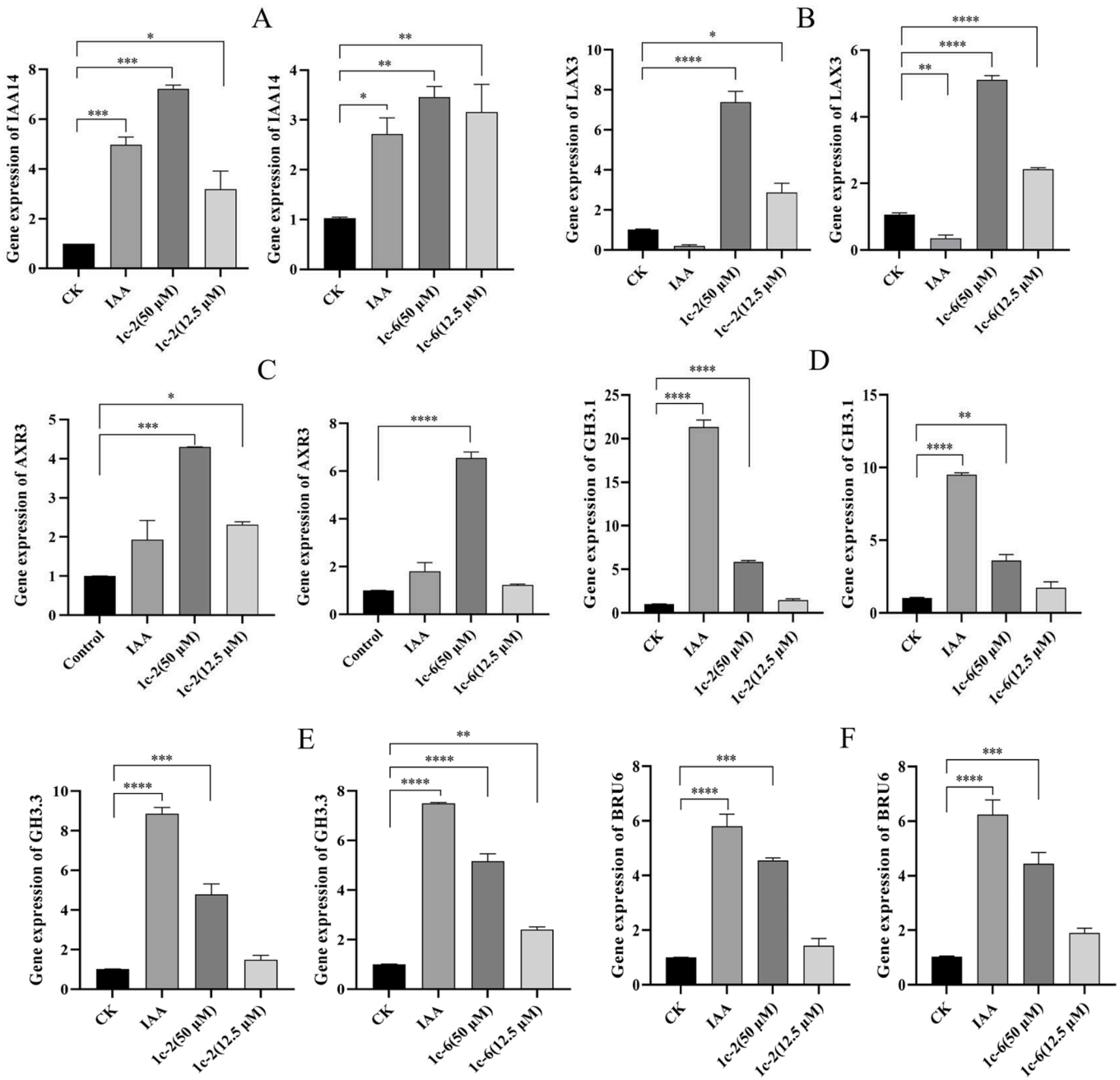

Fig. 7. QRT-PCR expression analysis of auxin pathway-related genes. P indicates significant difference (*p < 0.05, **p < 0.01, ***p < 0.001, ****p < 0.0001).

remodeling enzymes, which may aid in cell separation before the development of lateral root primordia. *LAX3* also facilitates the emergence of lateral roots by promoting the separation of the epidermis and cortex (Swarup et al., 2008).

The *AXR3* gene was found to significantly up-regulate compounds **C2** and **C6** (Fig. 7**C**). The alleles *AXR3-1* and *AXR3-3* are associated with IAA-excessive phenotypes such as reduced elongation and a reduced number of root hairs (Leyser et al., 1996). As shown in Fig. 8, root hair initiation is controlled by the relative abundance of SHY2 (SHORT HYPOCOTYL 2) and *AXR3* in the cell. A stabilizing mutation in AXR3/IAA17 inhibits root hair development and elongation (Knox et al., 2003). The IAA17/AXR3 protein participates in root development, and the accumulation of its mutant variant, *AXR3-1*, which cannot bind auxin, leads to a severe root growth phenotype and agravitropism (Kubalová et al., 2024). These findings illustrate the involvement of the *AXR3* gene in regulating root hair development.

There are 19 *GH3* genes in *A. thaliana*, which play a crucial role in regulating plant development and growth hormone balance. Studies have shown that changes in the expression of these genes can have a significant impact on plant growth and development (Guo et al., 2022; Kong et al., 2022). Interestingly, it has been observed that the application of 10 μM of auxin can lead to an increase in the expression of *GH3.1* and *GH3.3* genes, while compounds **C2** and **C6** have similar effects to growth factors (Fig. 7**D and 7E**). Moreover, mutants lacking all eight *GH3* genes exhibit distinct phenotypes such as short roots, dense root hairs, and long hypocotyls and petioles (Guo et al., 2022). As shown in Fig. 8, the levels of phenylacetic acid (PAA) in *A. thaliana* have been linked to lateral root formation. *GH3* growth hormone amide synthase plays a role in regulating the ratio of IAA to PAA during plant development (Aoi et al., 2020). Furthermore, members of the *GH3* gene family encode acylamide synthetases that bind IAA to amino acids. Compounds **C2** and **C6** have been shown to up-regulate the *BRU6* gene

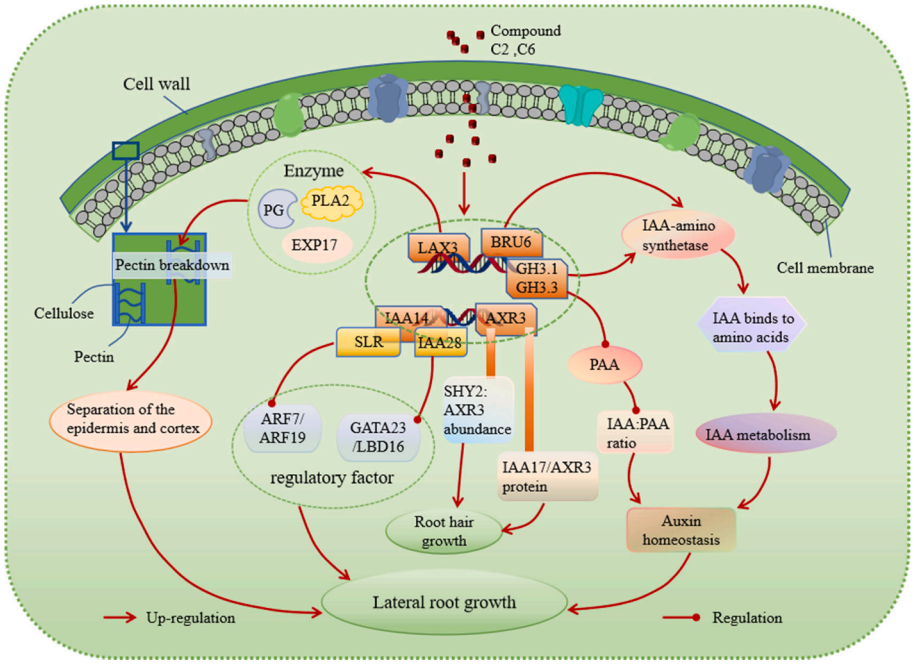

Fig. 8. The possible signalling pathway regulated by compound **C2** and **C6**.

(Fig. 7**F**) (Casanova-Sáez et al., 2022). The *GH3.1*, *GH3.3* and *BRU6* genes all encode IAA-amino synthases that catalyze the binding of IAA and amino acids to ensure local IAA homeostasis, thereby regulating plant growth (Zhao, 2018).

4. Conclusion

Nine *N*-thianyl indole acetamide derivatives were designed, synthesized, and tested for their effects on regulating root growth. The results indicated that *N*-thianyl indole acetamide derivatives showed a good inhibitory effect on the root growth of *A. thaliana,* with some compounds exhibiting a 100 % inhibition rate at 100 μM. Compounds **C2** and **C6** not only inhibited main root growth but also promoted the increase of lateral roots. They regulated the growth of *A. thaliana* lateral roots by regulating the expression of lateral root growth and development-related genes *IAA14*, *LAX3*, and *AXR3* in the auxin signaling pathway. Furthermore, they could also enhance the expression of IAA-amino synthetase-related genes *GH3.1*, *GH3.3*, and *BRU6*, catalyzing the combination of IAA and amino acids, ensuring the homeostasis of local auxin, and thereby regulating plant root growth.

5. Consent for publication

All authors consent to participate in the manuscript publication.

CRediT authorship contribution statement

Li Lei: Writing – original draft, Methodology, Investigation, Data curation. **Xu Tang:** Writing – review & editing, Validation. **Wei Sun:** Writing – review & editing, Validation. **Anjing Liao:** Writing – review & editing, Validation. **Jian Wu:** Funding acquisition, Formal analysis, Conceptualization.

Declaration of Competing Interest

The authors declare that they have no known competing financial interests or personal relationships that could have appeared to influence the work reported in this paper.

Acknowledgements

This work was supported by the National Key R&D Program of China (No. 2023YFD1700602), the Technology Achievement Transformation (general project) of Guizhou Province (Qiankehezhicheng[2024] the general 083, Qiankehechengguo [2022] the general 063), the Program of Introducing Talents to Chinese Universities (No. D20023), the Central Government Guides Local Science and Technology Development Fund Projects (Qiankehezhongyindi (2023) 001), Key Agricultural Technology R&D Projects of the Xinjiang Production and Construction Corps (NYHXGG, 2023AA602).

Appendix A. Supplementary material

Supplementary data to this article can be found online at https://doi.org/10.1016/j.arabjc.2024.106082.

References

Abercrombie, J.J., Leung, K.P., Chai, H., Hicks, R.P., 2015. Spectral and biological evaluation of a synthetic antimicrobial peptide derived from 1-aminocyclohexane carboxylic acid. Bioorg Med Chem 23, 1341–1347. https://doi.org/10.1016/J.BMC.2015.01.027.

Aoi, Y., Tanaka, K., Cook, S.D., Hayashi, K.I., Kasahara, H., 2020. GH3 auxin-amido synthetases alter the ratio of indole-3-acetic acid and phenylacetic acid in arabidopsis. Plant Cell Physiol 61, 596–605. https://doi.org/10.1093/PCP/PCZ223.

Bai, Y., Fernández-Calvo, P., Ritter, A., Huang, A.C., Morales-Herrera, S., Bicalho, K.U., Karady, M., Pauwels, L., Buyst, D., Njo, M., Ljung, K., Martins, J.C., Vanneste, S., Beeckman, T., Osbourn, A., Goossens, A., Pollier, J., 2021. Modulation of Arabidopsis root growth by specialized triterpenes. New Phytol 230, 228–243. https://doi.org/10.1111/NPH.17144.

Behazin, R., Ebrahimi, A., 2018. The physicochemical properties and tyrosinase inhibitory activity of ectoine and its analogues: A theoretical study. Comput Theor Chem 1130, 6–14. https://doi.org/10.1016/j.comptc.2018.03.003.

Beno, B.R., Yeung, K.-S., Bartberger, M.D., Pennington, L.D., Meanwell, N.A., 2015. A Survey of the Role of Noncovalent Sulfur Interactions in Drug Design. J Med Chem 58, 4383–4438. https://doi.org/10.1021/jm501853m.

Casanova-Sáez, R., Mateo-Bonmatí, E., Šimura, J., Pěnčík, A., Novák, O., Staswick, P., Ljung, K., 2022. Inactivation of the entire Arabidopsis group II GH3s confers tolerance to salinity and water deficit. New Phytol 235, 263–275. https://doi.org/10.1111/NPH.18114.

Clauss, A., Glaess, C., Marciniak, G., Nave, J.F., Vivet, B., 2010. Quinazoline-2,4(1H,3H)-dione derivatives, their preparation and use as phosphodiesterase, especially PDE7, inhibitors for treating inflammation, diabetes, psychiatric, neurological and cardiovascular diseases. WO2010116088.

Cosgrove, D.J., 2000. Loosening of plant cell walls by expansins. Nature 407, 321–326. https://doi.org/10.1038/35030000.
Dejonghe, W., Okamoto, M., Cutler, S.R., 2018. Small molecule probes of ABA biosynthesis and signaling. Plant Cell Physiol 59, 1490–1499. https://doi.org/10.1093/PCP/PCY126.
Fendrych, M., Akhmanova, M., Merrin, J., Glanc, M., Hagihara, S., Takahashi, K., Uchida, N., Torii, K.U., Friml, J., 2018. Rapid and reversible root growth inhibition by TIR1 auxin signalling. Nat Plants 4, 453–459. https://doi.org/10.1038/s41477-018-0190-1.
Ferro, N., Bredow, T., Jacobsen, H.J., Reinard, T., 2010. Route to novel auxin: auxin chemical space toward biological correlation carriers. Chem Rev 110, 4690–4708. https://doi.org/10.1021/CR800229S.
Frackenpohl, J., Abel, S.A.G., Alnafta, N., Barber, D.M., Bojack, G., Brant, N.Z., Helmke, H., Mattison, R.L., 2023. Inspired by nature: isostere concepts in plant hormone chemistry. J Agric Food Chem 71, 18141–18168. https://doi.org/10.1021/ACS.JAFC.3C01809.
Fu, J., Karur, S., Madera, A.M., Pecchi, S., Sweeney, Z.K., Tjandra, M., Yifru, A., 2014. Preparation of hydroxamic acid derivatives as LpxC inhibitors useful for the treatment of bacterial infection. WO2014160649.
Fukaki, H., Tameda, S., Masuda, H., Tasaka, M., 2002. Lateral root formation is blocked by a gain-of-function mutation in the SOLITARY-ROOT/IAA14 gene of Arabidopsis. Plant J 29, 153–168. https://doi.org/10.1046/J.0960-7412.2001.01201.X.
Fukaki, H., Nakao, Y., Okushima, Y., Theologis, A., Tasaka, M., 2005. Tissue-specific expression of stabilized SOLITARY-ROOT/IAA14 alters lateral root development in Arabidopsis. Plant J 44, 382–395. https://doi.org/10.1111/J.1365-313X.2005.02537.X.
Guo, R., Hu, Y., Aoi, Y., Hira, H., Ge, C., Dai, X., Kasahara, H., Zhao, Y., 2022. Local conjugation of auxin by the GH3 amido synthetases is required for normal development of roots and flowers in Arabidopsis. Biochem Biophys Res Commun 589, 16–22. https://doi.org/10.1016/J.BBRC.2021.11.109.
Guseman, J.M., Hellmuth, A., Lanctot, A., Feldman, T.P., Moss, B.L., Klavins, E., Calderón Villalobos, L.I.A., Nemhauser, J.L., 2015. Auxin-induced degradation dynamics set the pace for lateral root development. Development 142, 905–909. https://doi.org/10.1242/DEV.117234.
Hada, D., Sharma, K., 2018. Isolation and characterization of chemical compounds from fruit pulp of cassia fistula and their antimicrobial activity. J Drug Del Therap 8. https://doi.org/10.22270/JDDT.V8I2.1664.
Kast, J., Keil, M., Kolassa, D., Schirmer, U., Wuerzer, B., Meyer, N., Rademacher, W., Jung, J., 1988. Tetrahydro(thio)pyran-2,4-dione derivatives, procedure for their preparation, and their use as herbicides and plant growth regulators. DE3701298.
Knox, K., Grierson, C.S., Leyser, O., 2003. AXR3 and SHY2 interact to regulate root hair development. Development 130, 5769–5777. https://doi.org/10.1242/DEV.00659.
Kong, Q., Low, P.M., Lim, A.R.Q., Yang, Y., Yuan, L., Ma, W., 2022. Functional antagonism of WRI1 and TCP20 modulates GH3.3 expression to maintain auxin homeostasis in roots. Plants 11, 454. https://doi.org/10.3390/PLANTS11030454.
Kontani, T., Miyata, J., Hamaguchi, W., Kawano, T., Kamikawa, A., Suzuki, H., Sudo, K., 2005. Preparation of tetrahydro-2H-thiopyran-4-carboxamides as anti-herpesvirus agents. US20050032855.
Kubalová, M., Müller, K., Dobrev, P.I., Rizza, A., Jones, A.M., Fendrych, M., 2024. Auxin co-receptor IAA17/AXR3 controls cell elongation in Arabidopsis thaliana root solely by modulation of nuclear auxin pathway. New Phytol 241, 2448–2463. https://doi.org/10.1111/NPH.19557.
Łączkowski, K.Z., Biernasiuk, A., Baranowska-Łączkowska, A., Zielińska, S., Sałat, K., Furgała, A., Misiura, K., Malm, A., 2016. Synthesis, antimicrobial and anticonvulsant screening of small library of tetrahydro-2H-thiopyran-4-yl based thiazoles and selenazoles. J Enzyme Inhib Med Chem 31, 24–39. https://doi.org/10.1080/14756366.2016.1186020.
Lavenus, J., Goh, T., Roberts, I., Guyomarc'h, S., Lucas, M., De Smet, I., Fukaki, H., Beeckman, T., Bennett, M., Laplaze, L., 2013. Lateral root development in Arabidopsis: fifty shades of auxin. Trends Plant Sci 18, 450–458. https://doi.org/10.1016/J.TPLANTS.2013.04.006.
Leyser, H.M.O., Pickett, F.B., Dharmasiri, S., Estelle, M., 1996. Mutations in the AXR3 gene of Arabidopsis result in altered auxin response including ectopic expression from the SAUR-AC1 promoter. Plant J 10, 403–413. https://doi.org/10.1046/J.1365-313X.1996.10030403.X.
Li, S., Li, Q., Tian, X., Mu, L., Ji, M., Wang, X., Li, N., Liu, F., Shu, J., Crawford, N.M., Wang, Y., 2022. PHB3 regulates lateral root primordia formation via NO-mediated degradation of AUXIN/INDOLE-3-ACETIC ACID proteins. J Exp Bot 73, 4034–4045. https://doi.org/10.1093/JXB/ERAC115.
Livak, K.J., Schmittgen, T.D., 2001. Analysis of Relative Gene Expression Data Using Real-Time Quantitative PCR and the 2(-Delta Delta C(T)) Method. Methods 25, 402–408. https://doi.org/10.1006/meth.2001.1262.
Marín-Rodríguez, M.C., Orchard, J., Seymour, G.B., 2002. Pectate lyases, cell wall degradation and fruit softening. J Exp Bot 53, 2115–2119. https://doi.org/10.1093/JXB/ERF089.
Mustafa, M., Winum, J.Y., 2022. The importance of sulfur-containing motifs in drug design and discovery. Expert Opin Drug Discov 17, 501–512. https://doi.org/10.1080/17460441.2022.2044783.
Nigović, B., Kojić-Prodić, B., Antolić, S., Tomić, S., Puntarec, V., Cohen, J.D., 1996. Structural studies on monohalogenated derivatives of the phytohormone indole-3-acetic acid (auxin). Acta Crystallogr Sect B 52, 332–343. https://doi.org/10.1107/S010876819500838X.
Platts, J.A., Howard, S.T., Bracke, B.R.F., 1996. Directionality of hydrogen bonds to sulfur and oxygen. J Am Chem Soc 118, 2726–2733. https://doi.org/10.1021/JA952871S/SUPPL_FILE/JA2726.PDF.
Porter, W.L., Thimann, K.V., 1965. Molecular requirements for auxin action–I. Halogenated indoles and indoleacetic acid. Phytochemistry 4, 229–243. https://doi.org/10.1016/S0031-9422(00)86169-5.
Rademacher, W., 2015. Plant growth regulators: backgrounds and uses in plant production. J Plant Growth Regul 34, 845–872. https://doi.org/10.1007/S00344-015-9541-6.
Rajalakshmi, S., Sathiyarajeswaran, P., Samraj, K., Kanagavalli, K., 2020. A review on scopes, methods and rationale of integrative approach in siddha medicine with biomedicine. Int J Pharm Pharm Sci 6–11. https://doi.org/10.22159/IJPPS.2020V12I4.36973.
Sun, P., Huang, Y., Yang, X., Liao, A., Wu, J., 2023. The role of indole derivative in the growth of plants: a review. Front Plant Sci 13, 1120613. https://doi.org/10.3389/FPLS.2022.1120613.
Sun, P., Huang, Y., Chen, S., Ma, X., Yang, Z., Wu, J., 2024. Indole derivatives as agrochemicals: an overview. Chin Chem Lett 35, 109005. https://doi.org/10.1016/J.CCLET.2023.109005.
Swarup, K., Benková, E., Swarup, R., Casimiro, I., Péret, B., Yang, Y., Parry, G., Nielsen, E., De Smet, I., Vanneste, S., Levesque, M.P., Carrier, D., James, N., Calvo, V., Ljung, K., Kramer, E., Roberts, R., Graham, N., Marillonnet, S., Patel, K., Jones, J.D.G., Taylor, C.G., Schachtman, D.P., May, S., Sandberg, G., Benfey, P., Friml, J., Kerr, I., Beeckman, T., Laplaze, L., Bennett, M.J., 2008. The auxin influx carrier LAX3 promotes lateral root emergence. Nat Cell Biol 10, 946–954. https://doi.org/10.1038/NCB1754.
Tan, X., Calderon-Villalobos, L.I.A., Sharon, M., Zheng, C., Robinson, C.V., Estelle, M., Zheng, N., 2007. Mechanism of auxin perception by the TIR1 ubiquitin ligase. Nature 446, 640–645. https://doi.org/10.1038/NATURE05731.
Thimann, K.V., 1958. Auxin activity of some indole derivatives. Plant Physiol 33, 311–321. https://doi.org/10.1104/PP.33.5.311.
Vaidya, A.S., Helander, J.D.M., Peterson, F.C., Elzinga, D., Dejonghe, W., Kaundal, A., Park, S.Y., Xing, Z., Mega, R., Takeuchi, J., Khanderahoo, B., Bishay, S., Volkman, B. F., Todoroki, Y., Okamoto, M., Cutler, S.R., 2019. Dynamic control of plant water use using designed ABA receptor agonists. Science 366. https://doi.org/10.1126/SCIENCE.AAW8848.
Wahba, R.H., El-Sonbati, A.Z., Diab, M.A., Gomaa, E.A., AbouElleef, E.M., 2024. Electrochemical sensing of strontium ions cyclic voltammetry and investigation of rosemary extract's effects on their behavior: Antibacterial properties of rosemary extract and molecular docking analysis for potential COVID-19 therapeutic benefits. Microchem J 200, 110398. https://doi.org/10.1016/j.microc.2024.110398.
Wang, Y., Zhao, Z., Guo, R., Tang, Y., Guo, S., Xu, Y., Sun, W., Tu, H., Wu, J., 2024. Plant antiviral compounds containing pyrazolo [3,4-d] pyrimidine based on the systemin receptor model. Arab J Chem 17, 105849. https://doi.org/10.1016/J.ARABJC.2024.105849.
Zhang, R., Guo, S., Deng, P., Wang, Y., Dai, A., Wu, J., 2021. Novel ferulic amide Ac6c derivatives: design, synthesis, and their antipest activity. J Agric Food Chem 69, 10082–10092. https://doi.org/10.1021/ACS.JAFC.1C03892.
Zhang, Y., Ma, Y., Zhao, D., Tang, Z., Zhang, T., Zhang, K., Dong, J., Zhang, H., 2023. Genetic regulation of lateral root development. Plant Signal Behav 18, 2081397. https://doi.org/10.1080/15592324.2022.2081397.
Zhao, Y., 2010. Auxin biosynthesis and its role in plant development. Annu. Rev. Plant Biol. 61, 49–64. https://doi.org/10.1146/ANNUREV-ARPLANT-042809-112308.
Zhao, Y., 2018. Essential roles of local auxin biosynthesis in plant development and in adaptation to environmental changes. Annu Rev Plant Biol 69, 417–435. https://doi.org/10.1146/ANNUREV-ARPLANT-042817-040226.
Zhao, Z., Tu, H., Wang, Y., Yang, J., Hao, G., Wu, J., 2024. Chemical driving the subtype selectivity of phytohormone receptors is beneficial for crop productivity. J Agric Food Chem 72, 16583–16593. https://doi.org/10.1021/ACS.JAFC.4C04446.